Sonication Frequency of E. Coli Inactivation Employing Tensegrity Approach

Ahmad B. H. Kueh [1]

[1] Department of Civil Engineering, Faculty of Engineering, Universiti Malaysia Sarawak, Kota Samarahan, Sarawak, Malaysia

UNIMAS Water Centre (UWC), Faculty of Engineering, Universiti Malaysia Sarawak, Kota Samarahan, Sarawak, Malaysia

Email: [1] kbhahmad@unimas.my

Abstract

Bacterial infections persist to be a serious public health challenge, and effective techniques for their inactivation are essential. Effective sonic inactivation of bacteria like E. coli relies on identifying their resonant frequencies. However, traditional methods of discovering these frequencies through laborious physical experimentation can be time-consuming and costly. This article proposes a novel method for determining the resonant frequency of E. coli using a specially designed tensegrity model that incorporates spectral element formulation. The model, which conforms to the shape of E. coli, allows for the calculation of resonant frequencies without the need for time-consuming element sensitivity simulations. To overcome issues related to rigid body motion, a small incremental operation is employed to calculate the system determinant. The resonant frequencies obtained from the model are found to be in excellent agreement with available experimental results. Additionally, the model reveals that changes in E. coli geometry have a significant impact on inactivation frequency, while other parameters such as density are less influential. The proposed tensegrity model is a powerful technique that can provide rapid and accurate identification of resonant frequencies, making bacterial inactivation instantaneous and more effective, particularly during times of health crises.

Index Terms—E. coli, natural frequency, resonant, ultrasound inactivation.

1. Introduction

Ensuring drinking water security and cleanliness is of utmost importance to the essential survivability of humans worldwide. Various diseases due to water contamination by bacteria, viruses, and yeasts put great hazards on human health, especially in countries without proper water treatment facilities. Conventional water treatment methods in physical, chemical, or biological forms all present different limitations [1]–[7]. For instance, coagulation, aeration, and adsorption techniques have been exercised to remove pollutants or microbes from the water. The coagulation approach employs toxic coagulants like ferric chloride, aluminum sulfate, poly ferric sulfate, poly aluminum chloride, etc. thereby highly threatening the water quality. The aeration method is more difficult than the coagulation and adsorption due to the use of sequencing batch reactors, the process of which requires also high time consumption. The adsorption technique, though preferred, poses a new question of its long-standing impact due to the use of synthetic materials that is toxicity-relevant [1]. The employment of

chemicals in water treatment introduces an additional workload in handling their residual before the product can be consumed. Therefore, several alternatives have been proposed and continually improved to tackle these inadequacies.

It is discovered from scholarly works that the emerging sonification method has exhibited some promising outcomes in the decontamination events of bacterial and viral activities in various arenas like biomedicals, chemicals production, foods, drinks, and environment, especially where clean and disinfected surroundings are of enormous importance [8]–[10]. Sonication is the process of breaking down bacterial cells through the application of sound waves. The sound waves create pressure variations in the liquid medium that the bacteria are suspended in, leading to mechanical stress on the bacterial cells. This can cause damage to the cell membrane, leading to lysis or destruction of the bacterial cell walls, releasing the DNA contained within. The concept has been extensively used in the cleaning of medical laboratory instruments as well as food and drink processing equipment while proven beneficial in the inactivation of microorganisms, such as *Aureobasidium pullulans* [11], *Bacillus subtilis* [11]–[13], *Enterobacter aerogenes* [11], [14], *Escherichia coli* [12], [15], *Klebsiella pneumonia* [15], *Mycobacterium sp.* [16], and *Microcystis aeruginosa* [17], to name but a few.

Although the sonication method is highly attractive and to a certain extent effective, finding the right frequency to inactivate the microbes or diseased cells by experimental trials has proved to be both laborious and time-consuming. One fertile modeling technique able to describe satisfactorily with simplistic conduct the mechano-functions of microbes is by adopting the tensegrity model. Research advances in the past several years have evident the great capability of tensegrity models in describing a range of cell mechanical behaviors, including cell spreading, cell migration, cell detachment, mechano-sensation [18], etc.

Observing the ability to offer an accurate description of the tiny living bodies in various aspects, the tensegrity model is, therefore, employed in the current work for determining the resonant frequency of E. coli. The numerically determined resonant frequency narrows down the range needed for the inactivation of E. coli in the utilization of the sonication apparatus.

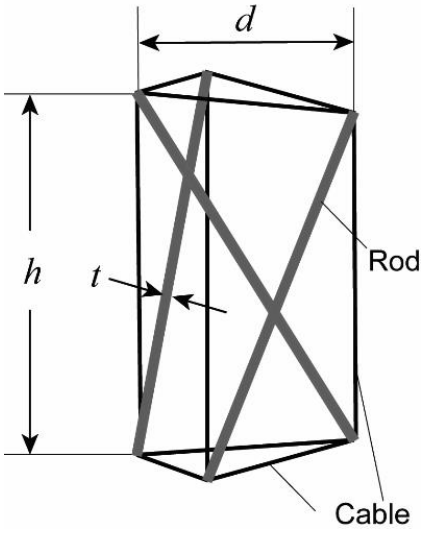

Fig. 1. E. coli tensegrity model

Table 1. Geometrical and material properties of E. coli

Property	Value	Reference
Length, h [μm]	0.3 – 6.0	[19]–[23]
Radius, r [μm]	0.25 – 1.0	[21], [24], [25]
Skin thickness, t [nm]	2 – 6	[26]
Density, ρ [g/mL]	0.19 – 1.1843	[27]–[29]
Young's modulus, E_g [MPa]	0.12 – 150	[26], [30], [31]

Further, a complexity-minimized modeling technique, from its methodology perspective to the details of the model, like the currently employed tensegrity model helps in facilitating economy in time, budgetary, and effort specifically at the events of parametric investigation, including variations in geometries and materials of the virus attributed to the dynamic nature and uncertainties that occurred in characterization.

2. Tensegrity modeling methodology

A. Geometrical and Mechanical Modeling Details

Single cell of E. coli is a complex biological body that comprises several constituents. Its main components include the cell wall, plasma membrane, cytoplasm, capsular wall, nucleoid, pili, ribosome, and flagellum. For the tensegrity model construction, the chief geometrical details required are the cell length, diameter, and skin thickness (measured from the outer capsular wall to plasma membranes) by its assumed rod shape. To characterize E. coli cells mechanically, overall Young's modulus and density are of concern. Table 1 summarizes the relevant geometrical and material properties stated above for the tensegrity model. Fig. 1 schematizes the tensegrity model as adopted from the triplex variant to represent the E. coli cell. The tensegrity model consists of 12 members: 3 rods to handle compressive forces as well as top and bottom sets of triangulated 6 cables plus the outer 3 vertically inclined cables for tensile forces.

Note that ρ and E_g in Table 1 are global properties measured for the whole E. coli cell. Tensegrity is typically a lattice-like structure comprising tension-resisting cables and compression-handling rods. Hence, these global properties are first converted to the equivalent local member properties. These are then used to prescribe the material characteristics of members of tensegrity. For brevity, Young's modulus and density of a member of the tensegrity model can be expressed, respectively, as

$$E_m = \frac{8}{3}\frac{\pi E_g r t}{A\left(\sqrt{2}+4\right)} \tag{1}$$

and

$$\rho_m = \frac{\rho}{16} \tag{2}$$

where A is the cross-sectional area of each member. The coordinates of tensegrity can be determined using the following.

x-coordinates:

$$x = \left\{ r \quad -r\cos\left(\frac{\pi}{3}\right) \quad -r\cos\left(\frac{\pi}{3}\right) \quad -r\sin\left(\frac{\pi}{3}\right) \quad 0 \quad r\sin\left(\frac{\pi}{3}\right) \right\}^T \tag{3}$$

y-coordinates:

$$y = \left\{ 0 \quad r\sin\left(\frac{\pi}{3}\right) \quad -r\sin\left(\frac{\pi}{3}\right) \quad r\cos\left(\frac{\pi}{3}\right) \quad -r \quad r\cos\left(\frac{\pi}{3}\right) \right\}^T \tag{4}$$

z-coordinates:

$$z = \{0 \quad 0 \quad 0 \quad h \quad h \quad h\}^T \tag{5}$$

B. Spectral Element Model Formulation

The definition of the tensegrity members exhibited in Fig. 1 is formulated employing the spectral element technique. It has been chosen attributed to its superiority to the finite element method (FEM) in evaluating the resonant frequency of a structure. FEM does not cover all important high-frequency wave modes unless a high element number is provided through fine discretization. It is owing to its formulation that relies on the frequency of independent polynomial shape functions used. This jeopardizes its accuracy, more so at high frequencies, which are short wavelengths relevant.

The weak form of governing equation for the frequency domain is first expressed as [32], [33]

$$\int_{\mathbf{0}}^{\boldsymbol{L}} \delta d[-\omega^2 \rho A d - F_x d'' - F(x)]dx = 0 \tag{6}$$

Integrating by parts leads the weak form to

$$\int_0^L [-\omega^2 \rho A d\delta d + F_x d'\delta d']dx - \delta d F(x)|_0^L - \int_0^L \delta d F(x)dx = 0 \tag{7}$$

Substitution of the dynamic shape functions into (7) yields

$$\left\{ \int_0^L [-\omega^2 \rho A \boldsymbol{F}^T \boldsymbol{F} + F_x \boldsymbol{F}'^T \boldsymbol{F}']dx \right\} \boldsymbol{d} = (\boldsymbol{f}_a + \boldsymbol{f}_b) \tag{8}$$

from which $\boldsymbol{f}_a$ is the spectral nodal forces vector

$$\boldsymbol{f_a} = \{f_1 \quad f_2\}^T = \{-f(0) \quad f(L)\}^T \tag{9}$$

and

$$\boldsymbol{f}_b = \int_0^L F(x)\boldsymbol{F}^T(x;\omega)dx \tag{10}$$

The spectral element stiffness equation for one element from (8) can be expressed as

$$\boldsymbol{S}(\omega)\boldsymbol{d} = \boldsymbol{f}(\omega) \tag{11}$$

where

$$\boldsymbol{S}(\omega) = \int_0^L [-\omega^2 \rho A \boldsymbol{F}^T \boldsymbol{F} + F_x \boldsymbol{F}'^T \boldsymbol{F}']dx \tag{12}$$

whereas

$$\boldsymbol{f}(\omega) = \boldsymbol{f}_a(\omega) + \boldsymbol{f}_b(\omega) \tag{13}$$

The spectral element equation in matrix form is written as

$$\boldsymbol{S}(\omega) = \begin{bmatrix} S_{11} & S_{12} \\ S_{21} & S_{22} \end{bmatrix} \tag{14}$$

where

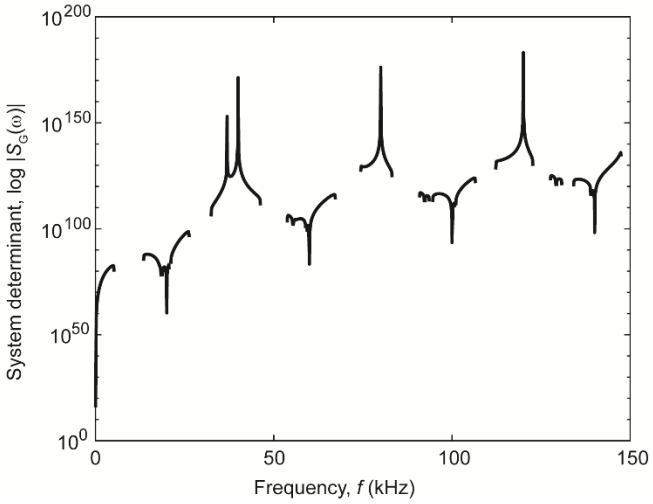

Fig. 2. Determinant of $S_G(\omega)$ vs frequency

Table 2. Verification of present tensegrity model with references

Existing work f_{res} [kHz]	Current f_{res} determination [kHz]	Difference [%]
20.0 [34]	20.0	0.0
20.0 [35]	20.0	0.0
30.0 [19]	30.02	0.07

$$S_{ij} = -F_x\alpha_{ij} - A\omega^2\rho\beta_{ij}, \quad i,j = 1,2 \tag{15}$$

with

$$\alpha_{11} = \frac{(k_1^2+k_2^2)L}{(e_2-e_1)^2},$$

$$\alpha_{12} = \alpha_{21} = \frac{-(e_2k_1^2+e_1k_2^2)L}{(e_2-e_1)^2},$$

$$\alpha_{22} = \frac{(e_2^2k_1^2+e_1^2k_2^2)L}{(e_2-e_1)^2},$$

$$\beta_{11} = \frac{(e_1^2+e_2^2)L}{(e_2-e_1)^2}, \quad \beta_{12} = \beta_{21} = \frac{-(e_1+e_2)L}{(e_2-e_1)^2}, \qquad \beta_{22} = \frac{2L}{(e_2-e_1)^2}, \tag{16}$$

by noting that

$$e_i = e^{-ik_iL}, \quad i,j = 1,2 \tag{17}$$

and

$$k_{1,2} = \pm\omega\sqrt{\frac{\rho A}{F_x}} \tag{18}$$

The transformation of the spectral element matrix equation from local to global definitions is performed employing the coordinate transformation matrix where the global system is expressed as (as opposed to that of local in (11))

$$\overline{\boldsymbol{S}}(\omega)\overline{\boldsymbol{d}} = \overline{\boldsymbol{f}}(\omega) \tag{19}$$

from which [36], [37]

$$\overline{\boldsymbol{S}}(\omega) = \boldsymbol{T}^{\boldsymbol{T}}\boldsymbol{S}(\omega)\boldsymbol{T} \tag{20}$$

where $\overline{\boldsymbol{d}}$ and $\overline{\boldsymbol{f}}(\omega)$are the transformed displacement and force vectors, respectively. Next, the spectral elemental matrix can be written as

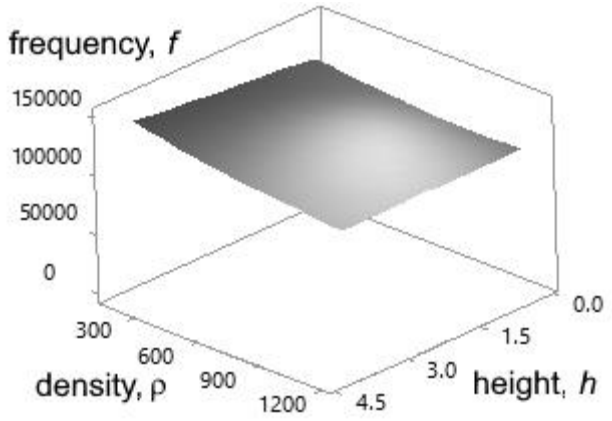

(a)

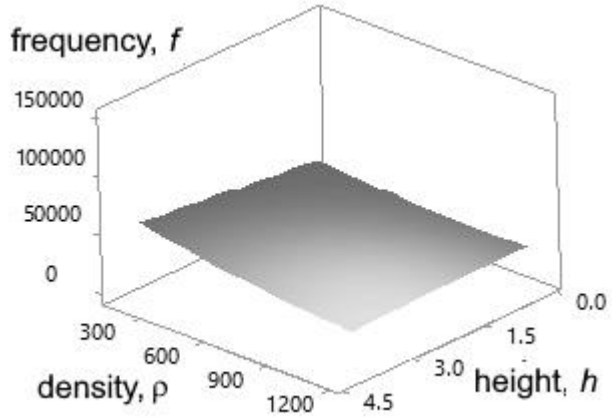

(b)

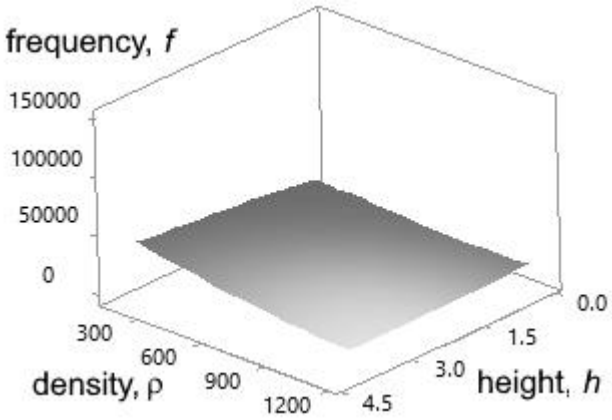

(c)

Fig. 3 Variation in the resonant frequency of E. coli for changes in h and ρ at E_g = 25 MPa for (a) r = 0.25 μm, (b) r = 0.625 μm, and (c) r = 1 μm. Note: h in μm, ρ in fg/μm^3, and f in Hz in the plots

$$\boldsymbol{S}(\omega) = \begin{bmatrix} 0 & 0 & 00 & 0 & 0 \\ 0 & S_{11} & 00 & S_{12} & 0 \\ 0 & 0 & 00 & 0 & 0 \\ 0 & 0 & 00 & 0 & 0 \\ 0 & S_{21} & 00 & S_{22} & 0 \\ 0 & 0 & 00 & 0 & 0 \end{bmatrix} \quad (21)$$

and the transformation matrix [T] is [38]

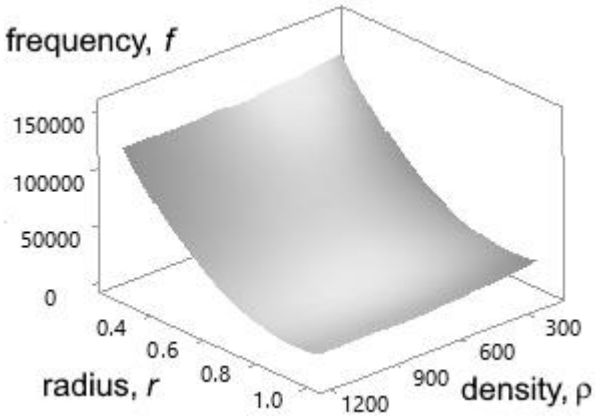

(a)

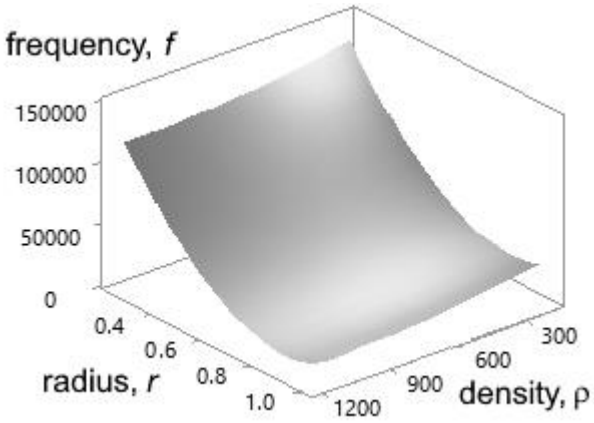

(b)

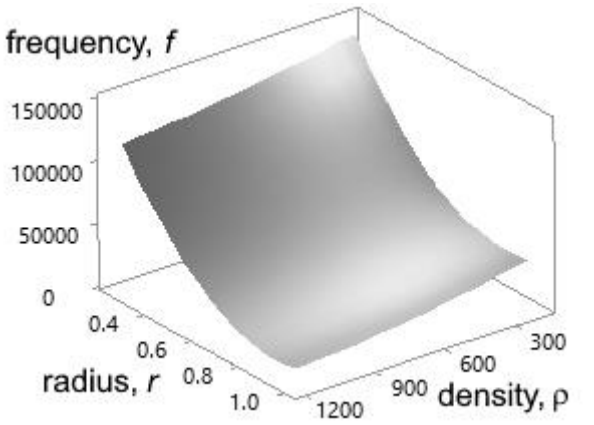

(c)

Fig. 4. Variation in the resonant frequency of E. coli for changes in r and ρ at E_g = 25 MPa for (a) h = 0.3 μm, (b) h = 2.15 μm, and (c) h = 4 μm. Note: r in μm, ρ in fg/μm^3, and f in Hz in the plots

$$\boldsymbol{T} = \begin{bmatrix} r_1 & r_2 & r_3 & 0 & 0 & 0 \\ s_1 & s_2 & s_3 & 0 & 0 & 0 \\ t_1 & t_2 & t_3 & 0 & 0 & 0 \\ 0 & 0 & 0 & r_4 & r_5 & r_6 \\ 0 & 0 & 0 & s_4 & s_5 & s_6 \\ 0 & 0 & 0 & t_4 & t_5 & t_6 \end{bmatrix} \quad (22)$$

r_i, s_i, and t_i are the directional cosines of the local degrees of freedom with respect to the global coordinate system. The assembly of (19) for each member is carried out by matching the number of degrees of freedom in the global coordinate system as

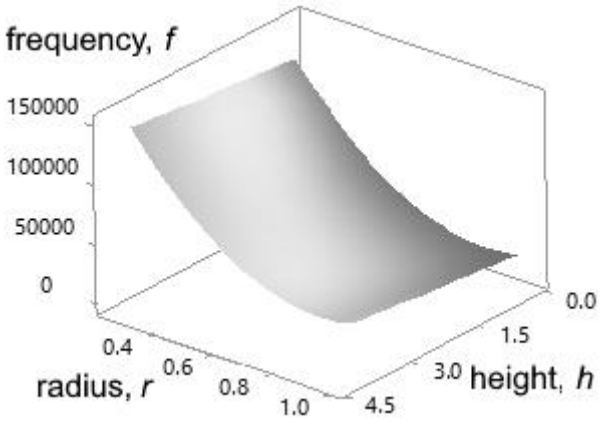

(a)

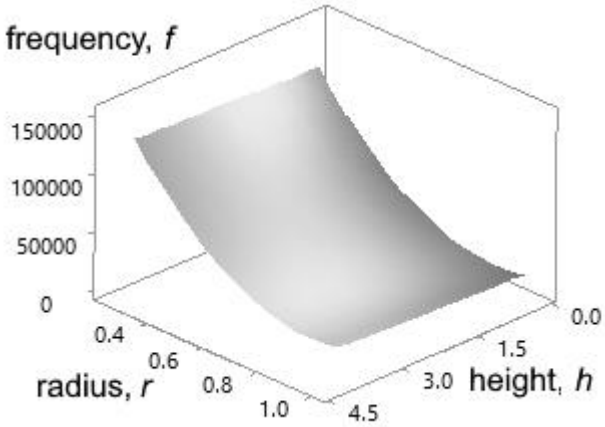

(b)

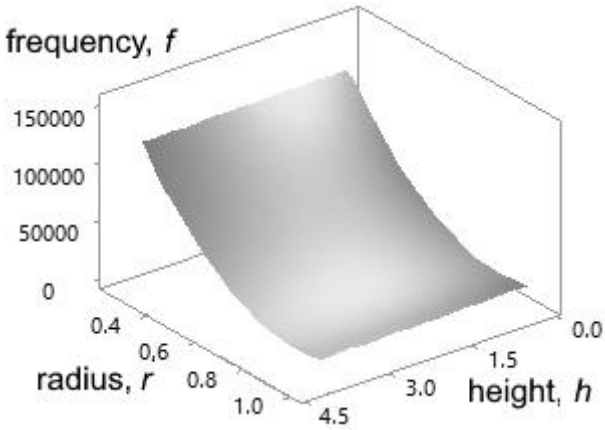

(c)

Fig. 5 Variation in the resonant frequency of E. coli for changes in r and h at E_g = 25 MPa for (a) ρ = 190 fg/μm^3, (b) ρ = 687.15 fg/μm^3, and (c) ρ = 1184.3 fg/μm^3. Note: r and h in μm, and f in Hz in the plots

$$\boldsymbol{S_G}(\omega)\boldsymbol{d_G} = \boldsymbol{f_G}(\omega) \quad (23)$$

The natural frequencies of the model are determined by setting the determinant of the global system to zero.

$$|\boldsymbol{S_G}(\omega)| = 0 \quad (24)$$

A tensegrity global dynamic matrix system tends to singularity to fulfill (24) so the common determinant can be problematic. Thus, a small incremental operation proposed by [39] to attain the system determinant that tends to zero is adopted.

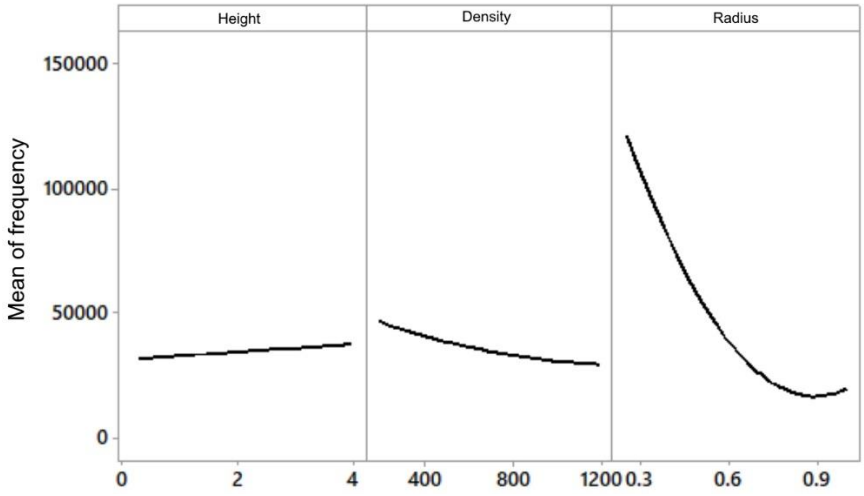

Fig. 6. Main effects of each factor on *f* (Hz)

3. Results and Discussion

A. Verification

The formulated and constructed tensegrity model is first used to compute the first natural frequency that causes resonance using the geometrical and material details from literature. From the diverse geometrical and material details collected from each paper, a sample of the real component of the determinant of $S_G(\omega)$ vs frequency plot is presented in Fig. 2 for E. coli studied in [34]. The resonant frequency, f_{res}, for the examined E. coli is attained from the frequency that locates the first major valley in the figure, i.e., f_{res} = 20 kHz. Table 2 lists the determined frequencies by the present tensegrity model vs. those of references [19], [34], [35]. It can be witnessed that the current model can predict accurately the resonant frequency used to inactivate different types of E. coli examined from the existing literature. The agreements are close. Therefore, the potency of the tensegrity model is evident.

B. Parametric Exploration

As properties of E. coli cells vary a great deal from one source to another, as can be observed in Table 1, it is worthwhile to interpret the resonant frequencies parametrically focusing on the upper and lower bounds gathered from the literature. An analysis of variance (ANOVA) has been executed for the lengths, radiuses, and densities found from these sources [40], [41]. Since many works show dominantly the global Young's moduli of the cell are approximately 25 MPa, this parameter has been set constant.

The effects of the variation of numerous factors (h, r, and ρ) on f, in which one of the terms is fixed, can be observed in Fig. 3. The ranges from Table 1 have been limited to h = 0.3 – 4 μm, r = 0.25 – 1 μm, ρ = 190 – 1184.3 fg/μm^3. Figs. 3(a), (b), and (c), Figs. 4(a), (b), and (c), as well as Figs. 5(a), (b), and (c) are plotted by fixing r, h, and ρ to a minimum, mid, and maximum of the ranges, respectively. Varying either h or ρ does not affect much the

computed *f*. The huge influence of *r* can be observed in the global elevation of the surface response in Figs. 3(a), (b), and (c) where varying *h* or ρ will not infer much effect as can be seen in the almost flat condition of the plots. The significance of *r* can also be noticed in Figs. 4(a), (b), and (c), as well as Figs. 5(a), (b), and (c), in which a rise in *r* changes the response surface in a declining manner whereas varying *h* or ρ inflicts a relatively much lesser effect in the resulted response in *f*. The major influence of *r* on *f* can be extracted and seen in Fig. 6. Again, *h* or ρ affect comparatively little the resonant frequency of E. coli. Besides, it can be learned that *r* and ρ show an inverse correlation with *f*, even more so as affected by *r*. Though slightly influenced, *f* increases with *h*.

4. Conclusion

The resonant frequencies of E. coli with various geometrical and material properties have been determined numerically using the tensegrity model adopting the spectral element formulation. It is presented that the model can accurately predict the resonant frequencies by comparing them with existing literature results. From ANOVA, it was determined that the geometrical parameter, specifically the cell radius, influences significantly the resonant frequency of E. coli. Its density contributes with a somewhat lower effect secondly. When other parameters are fixed, the resonant frequency of E. coli increases following a drop in its radius and density while a rise in length produces the same outcome only slightly. It is found that the radius of E. coli affects most significantly the resonant frequency used to inactivate the bacteria. The current technique can be extrapolated to other harmful bacteria in the events of drinking water treatment as well as medical and laboratory equipment disinfection.

5. Acknowledgment

The author thanks the Ministry of Higher Education, Malaysia (*Kementerian Pendidikan Tinggi Malaysia*) for the research fund under the Fundamental Research Grant Scheme (FRGS) (Grant number: FRGS/1/2020/TK0/UNIMAS/02/10). Research facilities and supports offered by Universiti Malaysia Sarawak are also greatly appreciated.

References

[1] A. Syafiuddin, S. Salmiati, T. Hadibarata, A. B. H. Kueh, M. R. Salim, and M. A. A. Zaini, "Silver nanoparticles in the water environment in Malaysia: Inspection, characterization, removal, modeling, and future perspective," *Sci. Rep.*, vol. 8, no. 1, p. Article 986, 2018, doi: 10.1038/s41598-018-19375-1.

[2] A. Syafiuddin, T. Hadibarata, A. B. H. Kueh, and M. Razman Salim, "Novel weed-extracted silver nanoparticles and their antibacterial appraisal against a rare bacterium from river and sewage treatment plan," *Nanomaterials*, vol. 8, no. 1, pp. 1–9, 2018, doi: 10.3390/nano8010009.

[3] Z. Z. Loh *et al.*, "Shifting from conventional to organic filter media in wastewater biofiltration treatment: A review," *Appl. Sci.*, vol. 11, no. 18, p. 8650, 2021, doi: 10.3390/app11188650.

[4] A. Ratnasari, A. Syafiuddin, A. B. H. Kueh, S. Suhartono, and T. Hadibarata, "Opportunities and challenges for sustainable bioremediation of natural and synthetic estrogens as emerging water contaminants using bacteria, fungi, and algae," *Water, Air, Soil Pollut.*, vol. 232, no. 6, pp. 1–23, 2021, doi: 10.1007/s11270-021-05183-3.

[5] D. N. A. Chee, F. Aziz, A. F. Ismail, A. B. H. Kueh, M. A. M. Amin, and M. Amran, "Adsorptive zeolitic imidazolate framework-8 membrane on ceramic support for the removal of lead(II) ions," *Chem. Eng. Sci.*, vol. 276, p. 118775, 2023, doi: 10.1016/j.ces.2023.118775.

[6] K. A. M. Said *et al.*, "Impact of montmorillonite clay on polysulfone mixed matrix membrane for heavy metal adsorption," *Water. Air. Soil Pollut.*, vol. 234, p. 275, 2023, doi: 10.1007/s11270-023-06275-y.

[7] K. A. M. Said *et al.*, "Methylene blue adsorption mechanism onto palm kernel shell-derived activated carbon: from particle diffusion to site adsorption," *BioResources*, vol. 18, no. 3, pp. 5120–5132, 2023, doi: 10.15376/biores.18.3.5120-5132.

[8] M. Kurokawa, P. M. King, X. Wu, E. M. Joyce, T. J. Mason, and K. Yamamoto, "Effect of sonication frequency on the disruption of algae," *Ultrason. Sonochem.*, vol. 31, pp. 157–162, 2016, doi: 10.1016/j.ultsonch.2015.12.011.

[9] C. Liu, J. Wang, Z. Cao, W. Chen, and H. Bi, "Variation of dissolved organic nitrogen concentration during the ultrasonic pretreatment to Microcystis aeruginosa," *Ultrason. Sonochem.*, vol. 29, pp. 236–243, 2016, doi: 10.1016/j.ultsonch.2015.09.017.

[10] X. Tan, D. Zhang, K. Parajuli, S. Upadhyay, Y. Jiang, and Z. Duan, "Comparison of four quantitative techniques for monitoring microalgae disruption by low-frequency ultrasound and acoustic energy efficiency," *Environ. Sci. Technol.*, vol. 52, no. 5, pp. 3295–3303, 2018, doi: 10.1021/acs.est.7b05896.

[11] S. Gao, Y. Hemar, M. Ashokkumar, S. Paturel, and G. D. Lewis, "Inactivation of bacteria and yeast using high-frequency ultrasound treatment," *Water Res.*, vol. 60, pp. 93–104, 2014, doi: 10.1016/j.watres.2014.04.038.

[12] S. Vajnhandl, T. Željko, A. Majcen Le Marechal, and J. V. Valh, "Feasibility study of ultrasound as water disinfection technology," *Desalin. Water Treat.*, vol. 55, no. 5, pp. 1393–1399, 2015, doi: 10.1080/19443994.2014.927331.

[13] H. Zou and L. Wang, "The disinfection effect of a novel continuous-flow water sterilizing system coupling dual-frequency ultrasound with sodium hypochlorite in pilot scale," *Ultrason. Sonochem.*, vol. 36, pp. 246–252, 2017, doi: 10.1016/j.ultsonch.2016.11.041.

[14] S. Gao, Y. Hemar, G. D. Lewis, and M. Ashokkumar, "Inactivation of Enterobacter aerogenes in reconstituted skim milk by high-and low-frequency ultrasound," *Ultrason. Sonochem.*, vol. 21, no. 6, pp. 2099–2106, 2014, doi: 10.1016/j.ultsonch.2013.12.008.

[15] E. Joyce, A. Al- Hashimi, and T. J. Mason, "Assessing the effect of different ultrasonic frequencies on bacterial viability using flow cytometry," *J. Appl. Microbiol.*, vol. 110, no. 4, pp. 862–870, 2011, doi: 10.1111/j.1365-2672.2011.04923.x.

[16] A. Al Bsoul, J.-P. Magnin, N. Commenges-Bernole, N. Gondrexon, J. Willison, and C. Petrier, "Effectiveness of ultrasound for the destruction of Mycobacterium sp. strain (6PY1)," *Ultrason. Sonochem.*, vol. 17, no. 1, pp. 106–110, 2010, doi: 10.1016/j.ultsonch.2009.04.005.

[17] Y. Li, X. Shi, Z. Zhang, and Y. Peng, "Enhanced coagulation by high-frequency ultrasound in Microcystis aeruginosa-laden water: Strategies and mechanisms,"

Ultrason. Sonochem., vol. 55, pp. 232–242, 2019, doi: 10.1016/j.ultsonch.2019.01.022.

[18] G. De Santis, A. B. Lennon, F. Boschetti, B. Verhegghe, P. Verdonck, and P. J. Prendergast, "How can cells sense the elasticity of a substrate?: an analysis using a cell tensegrity model," *Eur. Cell. Mater.*, vol. 22, pp. 202–213, 2011, doi: 10.22203/eCM.v022a16.

[19] N. M. Budari, M. F. Ali, K. H. Ku Hamid, K. A. Khalil, M. Musa, and N. F. Khairuddin, "Escherichia coli wild type cells disruption by low intensity ultrasound for bacterial disinfection," in *InCIEC 2015*, 2016, pp. 21–31, doi: 10.1007/978-981-10-0155-0_3.

[20] T. O. Ajiboye, S. O. Babalola, and D. C. Onwudiwe, "Photocatalytic inactivation as a method of elimination of E. coli from drinking water," *Appl. Sci.*, vol. 11, no. 3, p. 1313, 2021, doi: 10.3390/app11031313.

[21] F. Wu, A. Japaridze, X. Zheng, J. Wiktor, J. W. J. Kerssemakers, and C. Dekker, "Direct imaging of the circular chromosome in a live bacterium," *Nat. Commun.*, vol. 10, no. 1, pp. 1–9, 2019, doi: 10.1038/s41467-019-10221-0.

[22] M. R. Nurliyana *et al.*, "The detection method of Escherichia coli in water resources: A review," in *Journal of Physics: Conference Series*, 2018, vol. 995, no. 1, p. 12065, doi: 10.1088/1742-6596/995/1/012065.

[23] I. Gammoudi *et al.*, "Morphological and nanostructural surface changes in Escherichia coli over time, monitored by atomic force microscopy," *Colloids Surfaces B Biointerfaces*, vol. 141, pp. 355–364, 2016, doi: 10.1016/j.colsurfb.2016.02.006.

[24] S. T. Odonkor and J. K. Ampofo, "Escherichia coli as an indicator of bacteriological quality of water: An overview," *Microbiol. Res. (Pavia).*, vol. 4, no. 1, p. e2, 2013, doi: 10.4081/mr.2013.e2.

[25] Q. Cui *et al.*, "Validation of the mechano-bactericidal mechanism of nanostructured surfaces with finite element simulation," *Colloids Surfaces B Biointerfaces*, vol. 206, p. 111929, 2021, doi: 10.1016/j.colsurfb.2021.111929.

[26] J. C. Gumbart, M. Beeby, G. J. Jensen, and B. Roux, "Escherichia coli peptidoglycan structure and mechanics as predicted by atomic-scale simulations," *PLoS Comput. Biol.*, vol. 10, no. 2, p. e1003475, 2014, doi: 10.1371/journal.pcbi.1003475.

[27] C. L. Lewis, C. C. Craig, and A. G. Senecal, "Mass and density measurements of live and dead gram-negative and gram-positive bacterial populations," *Appl. Environ. Microbiol.*, vol. 80, no. 12, pp. 3622–3631, 2014, doi: 10.1128/AEM.00117-14.

[28] E. Martinez-Salas, J. A. Martin, and M. Vicente, "Relationship of Escherichia coli density to growth rate and cell age," *J. Bacteriol.*, vol. 147, no. 1, pp. 97–100, 1981, doi: 10.1128/jb.147.1.97-100.1981.

[29] J. Shiloach and R. Fass, "Growing E. coli to high cell density—a historical perspective on method development," *Biotechnol. Adv.*, vol. 23, no. 5, pp. 345–357, 2005, doi: 10.1016/j.biotechadv.2005.04.004.

[30] H. H. Tuson *et al.*, "Measuring the stiffness of bacterial cells from growth rates in hydrogels of tunable elasticity," *Mol. Microbiol.*, vol. 84, no. 5, pp. 874–891, 2012, doi: 10.1111/j.1365-2958.2012.08063.x.

[31] N. Kandemir, W. Vollmer, N. S. Jakubovics, and J. Chen, "Mechanical interactions between bacteria and hydrogels," *Sci. Rep.*, vol. 8, no. 1, pp. 1–11, 2018, doi: 10.1038/s41598-018-29269-x.

[32] S. H. Abo Sabah and A. B. H. Kueh, "Finite element modeling of laminated composite plates with locally delaminated interface subjected to impact loading," *Sci. World J.*, vol. 2014, p. Article 954070, 2014, doi: 10.1155/2014/954070.

[33] S. Q. Koo and A. B. H. Kueh, "Finite element state-space model of edge initiating localized interfacial degeneration of damped composite laminated plates," in *IOP Conference Series: Materials Science and Engineering*, 2019, vol. 620, no. 1, p. 012072, doi: 10.1088/1757-899X/620/1/012072.

[34] J. Li *et al.*, "Ultrasound-induced Escherichia coli O157: H7 cell death exhibits physical disruption and biochemical apoptosis," *Front. Microbiol.*, vol. 9, p. 2486, 2018, doi: 10.3389/fmicb.2018.02486.

[35] X. Liao *et al.*, "Multiple action sites of ultrasound on Escherichia coli and Staphylococcus aureus," *Food Sci. Hum. Wellness*, vol. 7, no. 1, pp. 102–109, 2018, doi: 10.1016/j.fshw.2018.01.002.

[36] A. B. H. Kueh, "Buckling of sandwich columns reinforced by triaxial weave fabric composite skin-sheets," *Int. J. Mech. Sci.*, vol. 66, pp. 45–54, 2013, doi: 10.1016/j.ijmecsci.2012.10.007.

[37] A. B. H. Kueh, "Thermally-induced responses of triaxially woven fabric composites," *Heliyon*, vol. 9, no. 7, p. e17631, 2023, doi: 10.1016/j.heliyon.2023.e17631.

[38] A. B. H. Kueh, "Fitting-free hyperelastic strain energy formulation for triaxial weave fabric composites," *Mech. Mater.*, vol. 47, pp. 11–23, 2012, doi: 10.1016/j.mechmat.2012.01.001.

[39] W. Wittrick and F. Williams, "A general algorithm for computing natural frequencies of elastic structures," *Q. J. Mech. Appl. Math.*, vol. 24, no. 3, pp. 263–284, 1971, doi: 10.1093/qjmam/24.3.263.

[40] A. B. H. Kueh, "Artificial neural network and regressed beam-column connection explicit mathematical moment-rotation expressions," *J. Build. Eng.*, vol. 43, p. 103195, 2021, doi: 10.1016/j.jobe.2021.103195.

[41] A. B. H. Kueh, A. W. Razali, Y. Y. Lee, S. Hamdan, I. Yakub, and N. Suhaili, "Acoustical and mechanical characteristics of mortars with pineapple leaf fiber and silica aerogel infills–measurement and modeling," *Mater. Today Commun.*, vol. 35, p. 105540, 2023, doi: 10.1016/j.mtcomm.2023.105540.